Quantum Electronics **49** (1) 25–28 (2019) ©2019 Kvantovaya Elektronika and Turpion Ltd

https://doi.org/10.1070/QEL16905

Bimodal imaging of functional changes in blood flow using optoacoustic and optical coherent angiography

A.G. Orlova, P.V. Subochev, A.A. Moiseev, E.O. Smolina,
S.Yu. Ksenofontov, M.Yu. Kirillin, N.M. Shakhova

Abstract. **The results of a complementary study of functional changes of the blood flow in human superficial tissues using optoacoustic (OA) microscopy and angiographic optical coherent tomography (OCT-A) during an occlusive test are demonstrated for the first time. OA microscopy data allow one to estimate the increase in blood content during the occlusive test, while OCT-A data demonstrate a decrease in the number of vessels with a functioning blood flow in the area of interest. The combined approach reported in the paper can be employed in experimental and clinical medicine to study the functional changes of microcirculation in diagnostics of vascular pathologies of superficial tissues and to evaluate the microcirculation response to treatment.**

Keywords: *optoacoustic microscopy, optical coherence tomography, angiography, functional test, cuff occlusion.*

1. Introduction

Morphofunctional changes in the microcirculatory bed of superficial tissues accompanying the development of a number of diseases are currently considered as approved or potential diagnostic criteria. Features of the vessel structure can serve as indicators of circulatory disorders in the diagnostics of dermatology, oncology, regenerative medicine, endocrinology, vascular and plastic surgery [1–5]. In clinical practice, a wide range of techniques are currently employed for noninvasive examination of skin microvasculature. To visualise the structure of blood vessels and assess the blood flow velocity, the capillaroscopy technique, which is characterised by a low imaging depth, and magnetic resonance imaging (MRI), which requires administration of contrasting agents, are employed. Laser Doppler anemometry/flowmetry techniques provide the estimation of the blood flow velocity; however, their drawbacks include low spatial resolution [6]. The laser speckle-flowmetry approach [7] based on the analysis of the dynamics of the speckle structure of scattered light when sensing the surface of a tissue with coherent radiation has a high potential for superficial tissue blood flow velocity mapping [7].

Recently, a significant progress was achieved in the development of optical and combined noninvasive imaging techniques providing three-dimensional visualisation of the microvascular bed in combination with functional diagnostics. Optoacoustic (OA) imaging is based on the registration of ultrasonic waves produced by the absorption of pulsed laser radiation by optical chromophores. OA visualisation combines the advantages of optical and acoustic approaches featuring both a high molecular contrast typical for optical techniques and a high (submillimetre) spatial resolution typical for ultrasound. Due to the high optical absorption of haemoglobin, OA techniques allow for high-contrast angiography [8].

Optical coherence tomography (OCT) is based on interferometric detection of the path length distribution of the photons backscattered on refractive-index inhomogeneities within the studied structures. A typical OCT device provides imaging of the internal structure of skin at depths up to 1–1.2 mm with a resolution of ~10 μm [9]. The Doppler OCT, based on the additional registration of the Doppler shift of photons forming the OCT image, provides complementary mapping of the blood flow direction and velocity distributions of in superficial skin layers [10]. However, a significant limitation of this technique consists in multiple scattering, resulting in distortion of the recorded velocity profiles [11]. Currently, a number of approaches have been proposed for contrasting the vessels basing on volumetric OCT imaging data [12–14]. Since the absolute majority of these approaches are based on detecting signal changes between consecutive OCT measurements, OCT-angiography (OCT-A) visualises primarily perfusion.

A parallel study of the vascular bed using OCT-A and OA allows obtaining simultaneously the information about the vessel structure, blood supply, as well as activity of blood flow. Since the physical principles of angiographic image formation in OA and OCT-A differ and these approaches have potential to be combined in a single device, the study of the feasibility of their complementary application in evaluating functional tissue responses is promising. This combination has already been used for sequential or simultaneous visualisation of the vascular bed of normal and scar tissue, as well as nevus, hemangioma, eczema, and basal cell carcinoma [15–18]. However, the complementary application of these techniques for the study of blood flow dynamics under external action has not been reported so far.

A wide range of functional tests based on a controlled effect on the tissue perfusion [6] are employed to assess the dynamic response of the vascular system and its alterations in case of various pathologies. The OA technique was for the first time proposed for evaluation of microcirculatory bed reaction during an occlusive test in the study [19]. The aim of present study is to assess the feasibility of the combined use of OCT-A and OA in the visualisation of functional

A.G. Orlova, P.V. Subochev, A.A. Moiseev, E.O. Smolina, S.Yu. Ksenofontov, M.Yu. Kirillin, N.M. Shakhova Institute of Applied Physics, Russian Academy of Sciences, ul. Ulyanova 46, 603950 Nizhny Novgorod, Russia; e-mail: orlova@ufp.appl.sci-nnov.ru

Received 30 October 2018; revision received 8 November 2018
Kvantovaya Elektronika **49** (1) 25–28 (2019)
Translated by M.Yu. Kirillin

changes in the vascular network of superficial skin layers under occlusion.

2. Materials and methods

2.1. Experimental OA setup

A Wedge HB532 pulsed laser (BrightSolutions, Italy) operating at a wavelength of 532 nm with a pulse repetition rate of 2 kHz and a pulse duration of 1 ns was used as a source of probe radiation in the experimental setup for OA angiography (IAP RAS, Russia). Three-dimensional images were acquired by mechanical scanning of the studied object with an optoacoustic head. Laser radiation was delivered to the head through a fibre-optic bundle, and the optoacoustic pulses produced in the medium were recorded with a single-element focused detector located in the centre of the head. The 35 MHz frequency band and the 6.7 mm focal distance of the acoustic detector ensured the spatial resolution of OA microscopy of 50 μm at depths up to 2 mm. To obtain OA images during the occlusive test, the sample was scanned in the lateral direction over the 3×3 mm area with a step of $\Delta x = \Delta y =$ 25 μm, thus providing the size of the OA image amounting 120×120 pixels. The total time for acquisition of the OA A-scans full set did not exceed 3 min [20].

To produce OA angiograms, the set of A-scans was processed using three numerical algorithms consequently applied to the initial data [21]. First, a one-dimensional deconvolution algorithm with Tikhonov regularisation [22] was applied to all A-scans, which allowed compensating the frequency-dependent acoustic absorption in the 35 MHz receiving frequency band of the OA antenna. At the next step, the two-dimensional Fourier reconstruction algorithm [23] was applied to all *xz* B-scans and *yz* B-scans, which allowed the OA antenna depth of field to increase from 0.75 mm to 2 mm. Finally, the three-dimensional Frangi filtering algorithm [24] was applied to the data after deconvolution and reconstruction, allowing an increase in the relative contrast of vascular (cylindrical) structures with a diameter between 7.5 μm and 200 μm (relative to spherical and flat structures of similar linear dimensions).

2.2. OCT-angiography

The OCT setup (IAP RAS, Russia) operates at a centre wavelength of 1.3 μm, and its axial and lateral resolutions amount 10 and 15 μm, respectively. The setup implements the principles of spectral OCT and is equipped with a spectrometer based on an InGaAs photodetector array (SU512-LD (512 Pixel), Sensors Unlimited, Inc., USA) providing 20000 in-depth scattering profile measurements (A-scans) per second. This allows one to record a volumetric array of 256×256×512 pixels, needed to visualise the vessels, in 26 seconds. Two-dimensional OCT scanning was performed in continuous mode, and the OCT scanner did not pass a single position twice. For vessel contrasting we employed an approach based on high-frequency finite impulse response filtering (HF FIR filter) in signal space [25]. Since scanning along the slow axis is performed with a significant (~60%) overlap of the scanning beam in adjacent measurements, the signal changes between adjacent measurements associated with motion have a larger high-frequency component compared to signal changes associated with the scanning process. Employment of HF FIR filtering allows one to calculate one OCT-A cross-sectional image (B-scan) based on only 7 neighbouring structural OCT B-scans and, thus, to visualise OCT-A B-scans in real time. Contrasting of the elongated structures in the images was performed using a two-dimensional filter [26], since the vessels in the 3D volume in the OCT-A are elongated in depth due to the so-called shadow artifact.

2.3. Occlusive test

The experiment on the complementary use of OA and OCT-A was conducted on a healthy 30-year-old male volunteer. During the experiment, the volunteer was sitting and placed his hand on a supporting plate, palm up; the hand was fixed, and the region of interest (ROI) was selected on the palm in the area of thenar. The size of the ROI was 3×3 mm, similar for OA and OCT-A. Temporary tissue clamping (cuff occlusion) was carried out using a compression cuff placed on the forearm approximately in the middle of the distance between the wrist and the elbow joint. In order to control the compression force, the pressure of the air pumped into the cuff was controlled and maintained in course of the test 60 mm Hg higher than the pre-measured systolic pressure of the volunteer. The study was conducted before compression, in 5 minutes after its beginning, and immediately after the release of the air from the cuff [27].

As a quantitative characteristic of the acquired angiographic images that allow one to evaluate the observed changes, the fraction of vessels in the tissue volume was selected. In OA images this value characterises blood content, while in OCT-A it shows the fraction of vessels with a functioning blood flow. To determine the vessels fraction in tissue volume, the 2D images of vascular networks obtained by OCT-A and OA methods were binarised. The ratio of the area occupied by the binarised vascular networks to the entire image area, expressed in percents, was considered as the vessels fraction in the image.

3. Results and discussion

Figure 1 shows the OA and OCT-A images of the microcirculatory bed of the same volunteer during the occlusive test. In OA images (Figs 1a–1c), haemoglobin-containing blood vessels are visualised against the background of the surrounding tissues as the areas with a high signal level. The large vessels are part of the deep skin plexus, while the small ones belong to the superficial plexus [28]. According to OA, in the studied palm area the vessels fraction in the entire tissue volume before occlusion amounts 52%.

OCT-A images (Figs 1d–1f), in turn provide perfusion imaging: high values correspond to the zones with the significant changes in the OCT signal value between two consequent measurements. Since OCT has a smaller imaging depth as compared to OA, only the vessels of the superficial plexus are visible in OCT-A images. According to OCT-A, the vessels fraction in the tissue volume is 28%. The lower value obtained by the OCT-A compared to OA can be explained by the lower probing depth and, hence, by the smaller contribution of large vessels.

The OA technique showed that under occlusion (Fig. 1b) the most pronounced changes in the OA signal occur in small vessels of the superficial plexus, which become temporarily filled with blood and, hence, clearly visible on OA images. For large vessels, an increase in the OA signal was also dem-

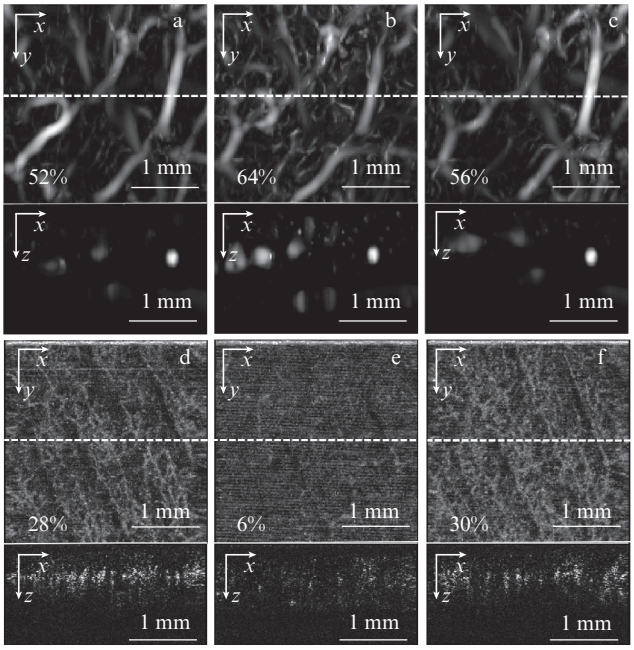

Figure 1. (a–c) OA and (d–f) OCT images of blood vessels of human palm (a, d) before occlusion, (b, e) during the occlusion, and (c, f) after occlusion. The top charts present C-scans (en-face view), and the bottom charts present B-scans (cross sections of vessels in depth *z*). Percentage values characterise the fraction of vessels in the entire tissue volume.

onstrated, indicating an increase in blood supply, which returned to the initial level after the release of the air from the cuff (Fig. 1c). The fraction of vessels in the tissue volume during and after the end of the clamping amounted 64% and 56%, respectively (Figs 1b and 1c). An increase in the haemoglobin content in the skin during vascular occlusion has already been demonstrated previously using optical [20, 29] and optoacoustic [30] techniques.

The OCT-A technique demonstrated that occlusion leads to a significant decrease in the intensity of blood flow manifested by the almost complete disappearance of the signal (Fig. 1e). The cessation of occlusion leads to the restoration of the blood flow [6], which can be indirectly observed in OCT-A images as an increase in the number of visible vessels (Fig. 1f). According to OCT-A, the fraction of vessels with a functioning blood flow during and after occlusion amounted 6% and 30%, respectively.

It should be noted that the spatial resolution of OA does not allow for imaging vascular structures located closer than 50 μm to each other, while OCT-A has a spatial resolution of ~10 μm (the employed setup has lateral and axial resolution of 15 μm and 10 μm, respectively), which allows more detailed images of the superficial plexus to be obtained, while the large OA imaging depth allows for visualisation of the structure of the skin deep plexus.

Compared to the setups previously employed for the complementary study of skin vessels [15–18], the OA microscope used in this work had an improved spatial resolution (50 μm) due to the more broadband antenna and a reduced diagnostic depth (2–3 mm) due to a shorter probe laser wavelength. The advantage of the OCT setup employed in this study consists in ability to visualise cross-sectional angiographic images in real time.

The combination of OCT-A and OA techniques made it possible to simultaneously trace changes in two microcirculation parameters: total haemoglobin and blood flow velocity. The results showing an increase in blood supply with a simultaneous decrease in perfusion during the occlusive test have already been demonstrated previously with the combination of optical diffuse spectroscopy and Doppler ultrasonography [31–32]; the results of this study are in good agreement with the cited papers. Given the fact that the reaction of microcirculatory system to occlusion is different in healthy tissues and in the case of peripheral arterial diseases [33–34], this approach can be efficiently employed for medical diagnostics purposes. In addition, the high resolution of the employed techniques allows visualising individual vessels, which can be additionally used to observe the anomalies of their structure.

4. Conclusions

Combined employment of OA and OCT-A techniques allowed us to obtain complementary information about the structural and functional changes in the microvasculature during the occlusive test. OA microscopy provided data for a quantitative assessment of the fraction of blood-containing vessels in the tissue volume and a qualitative evaluation of their shape and position. Angiographic OCT provided evaluation of the fraction of vessels with functioning blood flow in tissue.

Acknowledgements. Complementary *in vivo* study of tissues by OCT-A and OA techniques was supported by the Russian Foundation for Basic Research (Project No. 15-29-04884). The development of numerical algorithms used to obtain optoacoustic images was carried out under the support of Russian Science Foundation (Project No. 18-45-06006).

References

1. Rezvani H.R., Ali N., Nissen L.J., Harfouche G., de Verneuil H., Taieb A., Mazurier F. *J. Invest. Dermatol*., **131**, 1793 (2011).
2. Velasco P., Lange-Asschenfeldt B. *Br. J. Dermatol*., **147**, 841 (2002).
3. Sorg H., Tilkorn D.J., Hager S., Hauser J., Mirastschijski U. *Eur. Surg. Res*., **58**, 81 (2017).
4. Stirban A. *Curr. Diab. Rep*., **14**, 541 (2014).
5. Dusseldorp J.R., Pennington D.G. *Plast. Reconstr. Surg. Global Open,* **2**, e228 (2014).
6. Wright C.I., Kroner C.I., Draijer R. *J. Pharmacol. Toxicol. Meth.*, **54**, 1 (2006).
7. Nadort A., Kalkman K., van Leeuwen T.G., Faber D.J. *Sci. Rep*., **6**, 25258 (2016).
8. Mercep E., Deán-Ben X.L., Razansky D. *Photoacoustics*, **10**, 48 (2018).
9. Izatt J.A., Choma M.A., Dhalla A.H., in *Optical Coherence Tomography* (Springer, Cham, 2015) pp 65–94.
10. Chen Z., Milner T., Srinivas S., Wang X., Malekafzali A., van Gemert M.J.C., Nelson J.S. *Opt. Lett*., **22**, 1119 (1997).
11. Bykov A.V., Kirillin M.Yu., Priezzhev A.V. *Quantum Electron*., **35**, 1079 (2005) [*Kvantovaya Elektron*., **35**, 1079 (2005)].
12. Yu L., Chen Z. *J. Biomed. Opt*., **15**, 016029 (2010).
13. Mariampillai A., Standish B.A., Moriyama E.H., Khurana M., Munce N.R., Leung M.K., Jiang J., Cable A., Wilson B.C., Vitkin I.A. *Opt. Lett*., **33**, 1530 (2008).
14. Jonathan E., Enfield J., Leahy M.J. *J. Biophoton.*, **4**, 583 (2011).
15. Zabihian B., Weingast J., Liu M., Zhang E., Beard P., Pehamberger H., Drexler W., Hermann B. *Biomed. Opt. Express*, **6**, 3163 (2015).
16. Liu M., Chen Z., Zabihian B., Sinz C., Zhang E., Beard P.C., Ginner L., Hoover E., Minneman M.P., Leitgeb R.A., Kittler H., Drexler W. *Biomed. Opt. Express*, **7**, 3390 (2016).

17. Zabihian B., Chen Z., Rank E., Sinz C., Bonesi M., Sattmann H., Ensher J., Minneman M.P., Hoover E., Weingast J., Ginner L., Leitgeb R., Kittler H., Zhang E., Beard P., Drexler W., Liu M. *J. Biomed. Opt.*, **21**, 96011 (2016).
18. Chen Z., Rank E., Meiburger K.M., Sinz C., Hodul A., Zhang E., Hoover E., Minneman M., Ensher J., Beard P.C., Kittler H., Leitgeb R.A., Drexler W., Liu M. *Sci. Rep.*, **7**, 17975 (2017).
19. Favazza C.P., Cornelius L.A., Wang L.V. *J. Biomed. Opt.*, **16**, 026004 (2011).
20. Subochev P., Orlova A., Mikhailova I., Shilyagina N., Turchin I. *Biomed. Opt. Express*, **7**, 3951 (2016).
21. Subochev P., Perekatova V., Kirillin M., Orlova A., Smolina E., Loginova D., Turchin I. *Proc. Int. Conf. Laser Optics* (ICLO) (IEEE, 2018) p. 482.
22. Van de Sompel D., Sasportas L.S., Jokerst J.V., Gambhir S.S. *PLoS One*, **11**, e0152597 (2016).
23. Jaeger M., Schüpbach S., Gertsch A., Kitz M., Frenz M. *Inverse Problems*, **23**, S51 (2007).
24. Oruganti T., Laufer J.G., Treeby B.E. *Proc. SPIE*, **8581**, 85811W (2013).
25. Moiseev A., Ksenofontov S., Sirotkina M., Kiseleva E., Gorozhantseva M., Shakhova N., Matveev L., Zaitsev V., Matveyev A., Zagaynova E., Gelikonov V., Gladkova N., Vitkin A., Gelikonov G. *J. Biophotonics*, **11**, e201700292 (2018).
26. Zhang M., Hwang T.S., Campbell J.P., Bailey S.T., Wilson D.J., Huang D., Jia Y. *Biomed. Opt. Express*, **7**, 816 (2016).
27. Casavola C., Paunescu L.A., Fantini S., Gratton E. *J. Biomed. Opt.*, **5**, 269 (2000).
28. Weller R.P., Hunter J.A., Savin J.A., Dahl M.V. (Eds) *Clinical Dermatology* (Blackwell Publ., 2013) p. 364.
29. Nagashima Y., Yada Y., Hattori M., Sakai A. *Int. J. Biometeorol.*, **44**, 11 (2000).
30. Subochev P., Orlova A., Smolina E., Kirillov A., Shakhova N., Turchin I. *Laser Phys. Lett.*, **15**, 045602 (2018).
31. Strömberg T., Sjöberg F., Bergstrand S. *Microvasc. Res.*, **113**, 50 (2017).
32. Abay T.Y., Kyriacou P.A. *J. Clin. Monit. Comput.*, **32**, 447 (2018).
33. Khalil M.A., Kim H.K., Hoi J.W., Kim I., Dayal R., Shrikhande G., Hielscher A.H. *Eur. J. Vasc. Endovasc. Surg.*, **49**, 83 (2015).
34. Alomari M.A., Khabour O.F., Alawneh K., Shammaa R.A. *Int. J. Rheumatol.*, **2018**, 8498651 (2018).